Image-based Discrimination and Spatial Non-uniformity Analysis of Effect Coatings

Jiří Filip[1], Radomír Vávra[1], Frank J. Maile[2] and Bill Eibon[3]

[1]*The Czech Academy of Sciences, Institute of Information Theory and Automation, Prague, Czech Republic*
[2]*Schlenk Metallic Pigments, GmbH, Roth-Barnsdorf, Germany*
[3]*PPG Industries, Cleveland, Ohio, U.S.A.*

Abstract: Various industries are striving for novel, more reliable but still efficient approaches to coatings characterization. Majority of industrial applications use portable instruments for characterization of effect coatings. They typically capture a limited set of in-plane geometries and have limited ability to reliably characterize gonio-apparent behavior typical for such coatings. The instruments rely mostly on color and reflectance characteristics without using a texture information across the coating plane. In this paper, we propose image-based method that counts numbers of effective pigments and their active area. First, we captured appearance of eight effect coatings featuring four different pigment materials, in in-plane and out-of-plane geometries. We used a gonioreflectometer for fixed viewing and varying illumination angles. Our analysis has shown that the proposed method is able to clearly distinguish pigment materials and coating applications in both in-plane and out-of-plane geometries. Finally, we show an application of our method to analysis of spatial non-uniformity, i.e. cloudiness or mottling, across a coated panel.

1 INTRODUCTION

Coating industry uses a wide range of pigment materials in combination with physical principles to achieve eye-catching appearance of the coated surfaces that stand out from the crowd (Maile and Reynders, 2010). Metallic pigments rely mainly on geometrical properties of flakes and their reflectance, interference pigments introduce effects due to light wave interference with transparent substrate coated with materials of high refractive indices, and diffraction pigments decompose light at a diffraction grating of a frequency close to the wavelength of the incoming light. Note that in practice many effect coatings are often combinations of the above classes.

Majority of industrial and refinish aftermarket applications use portable instruments for characterization of effect coatings. They typically capture between 3 and 6 standard in-plane geometries for fixed illumination and variable observation angles. Such a limited set of capturing geometries restricts their ability to reliably characterize gonio-apparent behavior typical for effect coatings.

As an example can serve a car body refinishing in Fig. 1, where coating appearance of the front and

Figure 1: Example of a car body part visually different from the rest of body due to an insufficient number of illumination/viewing validation angles.

rear doors is not matched due to insufficient angular sampling.

Therefore, industries are striving for novel, more reliable but still efficient approaches to coatings characterization (Höpe et al., 2014). Majority of the methods rely mostly on color and reflectance characteristics. Spatial information is not commonly used in industrial instruments. Currently, only two of them can capture texture maps and use proprietary algorithm to derive the levels of sparkliness and graininess referring to coating properties under directional and diffuse illumination; however, their definitions and their relation to typical user observations are unknown.

One of the promising approaches to effect pig-

ments characterization is using complementary information about pigment flakes density, distribution and orientation in the coating layer. To this end, we perform this analysis using a gonioreflectometer for in-plane and out-of-plane geometries of fixed viewing and varying illumination angles. Next, we propose image-based coating characterization method that counts numbers of effective pigments and their coverage area. Our method allows robust discrimination of different pigment materials as well as the same material with different coating technology.

Our paper first discusses a prior work in the field in Section 2. Then the analyzed coating samples and acquisition method are introduced in Section 3. Method of pigment flakes detection is outlined in Section 4 and its results are given in Section 5. Application of the method to spatial uniformity analysis of coatings is presented in Section 6, while the Section 7 concludes the paper.

2 RELATED WORK

One of the first survey works on application of angle-dependent optical effects deriving from submicron structures of films and pigments was presented in (Pfaff and Reynders, 1999). A detailed overview of special effect pigments is given in (Maile et al., 2005) and (Pfaff, 2008).

Before considering to use any novel measurement geometries, one can validate current industrial standards (DIN (DIN, 1999) and ASTM (E2194-12, 2012),(E2539-12, 2012) used for the measurement of appearance stemming from past research of gloss and chromatic appearance (Hunter, 1937), (McCamy, 1996). This led to development of industrial multi-angle gonioreflectometers: MA68 and MA98 by X-rite, BYK-mac by Gardner, and MultiFX10 by Datacolor as described more in detail in (Perales et al., 2013). These devices typically capture between 5–12 in-the-plane geometries and BYK-mac even allows pigment texture measurement using a built-in camera. However, when it comes to effect coatings characterization, these devices, due to limited set of measurement geometries, often struggle to identify individual coatings reliably (Gómez et al., 2016).

A wide body of research work has been devoted to analysis of bidirectional reflectance distribution functions (BRDF) (Nicodemus et al., 1977) and chromatic properties of effect coatings. Different measurement geometries were analyzed in (Kirchner and Cramer, 2012), (Ferrero et al., 2015). A BRDF characterization of effect coatings using a half-difference parameterization of individual flakes was presented in

(Ferrero et al., 2013). The same parameterization was applied in (Strothkämper et al., 2016) to predict the global color appearance of coated surfaces and to analyze color estimation using multi-angle spectrophotometers (Ferrero et al., 2015). Characterization of diffraction pigments was studied in (Ferrero et al., 2016).

Method of BRDF measurement and modelling of effect coatings was introduced in (Mihálik and Ďurikovič, 2013). Kim et al. (Kim et al., 2010) proposed a novel image-based method of pearlescent paints spectral BRDF measurement using a dedicated goniometric setup relying on a spherical sample and derived a non-parametric bivariate reflectance model. Lans et al. (Lans et al., 2012) presented an empirical approach to the realistic modelling of special effect flakes fitting patch-based model parameters using sparse texture data obtained by a portable multi-angle spectrophotometer. In (Rump et al., 2009) were presented extensions towards gonioapparent coatings texture measurement and modelling using bidirectional texture function (BTF) (Dana et al., 1999).

Although this research advanced considerably an understanding of the processes driving the reflectance and chromatic appearance of effect coatings, we are not aware of any technique simultaneously analyzing both spatial and gonioapparent appearance of effect coatings at pigment size level.

3 COATING SAMPLES ACQUISITION

Effect pigments can be, based on the principle of chroma and sparkling effect generation, roughly divided into three categories (Maile et al., 2005): metallic, interference, and diffractive pigments. We tested eight effect coatings featuring four different pigment materials and different coating technology as shown in inset images in Fig. 2:

- *Polychromatic* (MultiFlect®) – a polychromatic coating including a diffraction pigment varying in liquefying agent (water - *poly1,poly3*, solvent - *poly2*) and its density (medium - *poly1*, *poly2* and high - *poly3*).

- *Ultra thin pigment* (Zenexo®) a high-sparkle contrast, pearlescent coating including an ultra-thin, colored aluminium pigment: *UTP*.

- *Aluminum* – coating including aluminum flakes of silverdollar morphology: solvent (*alu1*) and water-based (*alu2*).

- *Mica* – coating including white mica flakes flakes: solvent (*mica1*) and water–based (*mica2*).

(a) *polychromatic1*   (b) *polychromatic2*   (c) *polychromatic3*   (d) *UTP*

(e) *aluminum1*   (f) *aluminum2*   (g) *mica1*   (h) *mica2*
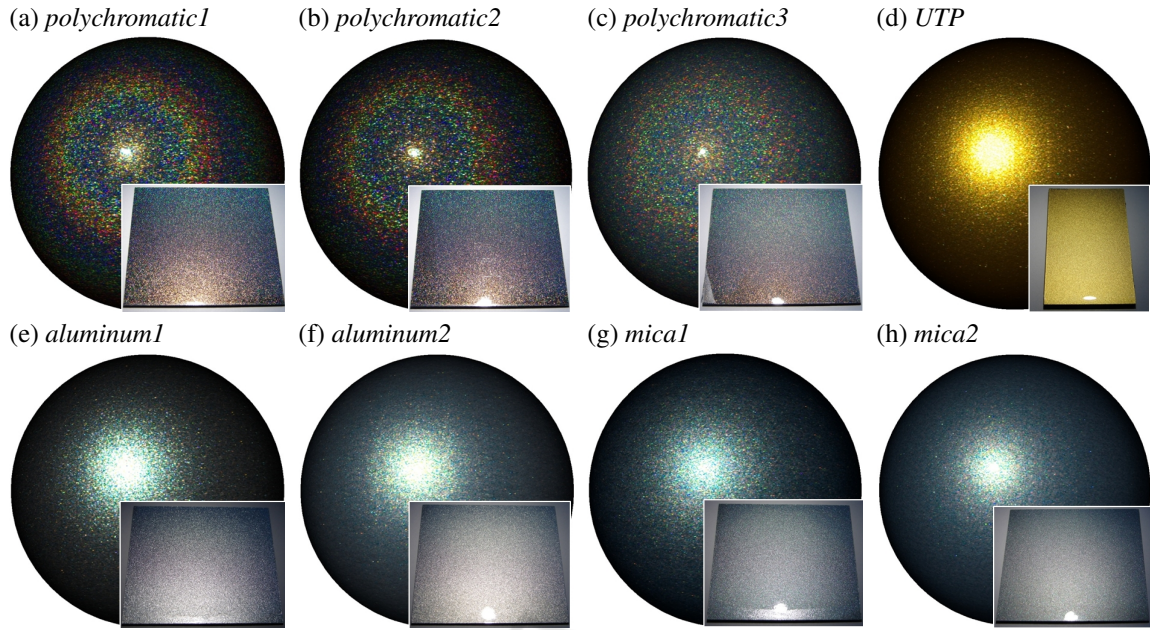
Figure 2: Photos (insets) of the tested coatings and their appearance captured as BTF visualized on a sphere: three samples containing polychromatic effect pigments (a,b,c), one sample with ultra-thin pigment (d), two samples using aluminum flakes (e,f), and two samples featuring white mica pigment (g,h).

All samples have comparable mean particle sizes ≈25 *μm*.

To capture the appearance of the tested effect coatings we used UTIA gonioreflectometer (Filip et al., 2013). It has four degrees of freedom (DOF) realized by a turntable with the measured sample (1 DOF) and by two arms: one holding a RGB camera (1 DOF), and one holding a LED light (2 DOF). The inner arm holds the LED light source 1.1m from the sample and produces a narrow and uniform beam of light. The outer arm holds an industrial, full-frame 16Mpix RGB camera AVT Pike 1600C. The sensor's distance from the sample is 2m. By combination of camera exposures and lighting intensities we capture high-dynamic-range RGB images of the coating, where a single pixel occupies approximately 46*μm*. The analyzed coating area was approximately 6x6mm. Appearance of the test coating captured as BTF is shown in Fig. 2

4 SPATIAL ANALYSIS OF EFFECT COATINGS

In order to identify the number of visible, i.e. active pigment flakes, in each image I, we performed the following analysis in each RGB channel. We decided to use RGB instead of common L*a*b as it is native colorspace of our camera and to avoid possible errors due

to a conversion process. First, we selected a candidate whose image pixels had distinct color in the particular color channel, e.g., for the red channel, the following conditions had to apply

$$(P_R > P_G + d) \ \& \ (P_R > P_B + d) \ , \qquad (1)$$

where P are pixel intensity values, $d = 0.2$, i.e., 20% of the image dynamic range and subscripts $_{R,G,B}$ denote individual color channels.

However, these conditions are insufficient in the center of the high-reflectance pigments, whose values often tend to be achromatic. Therefore, we extended the color information from the pixel's neighborhood by filtering the image I using a Gaussian filter (width 10 pixels, standard deviation $\sigma = 1.0$) to produce a filtered image I^F. The following alternative conditions were used

$$\begin{aligned} (P_R > m) \quad \& \quad (P_G > m) \quad \& \quad (P_B > m) \quad \& \dots \\ \& \quad (P_R^F > P_G^F) \quad \& \quad (P_R^F > P_B^F) \ , \quad (2) \end{aligned}$$

where P^F are pixels from filtered image and $m = 0.9$, i.e., 90% of the image dynamic range. The equations for the other two channels are similar.

If any of the above conditions for the tested pixel apply, the pixel becomes a candidate for a respective color channel. To remove visual noise outliers resulting from possible flakes interreflections, the image is the subject of a morphological opening operator, dis-
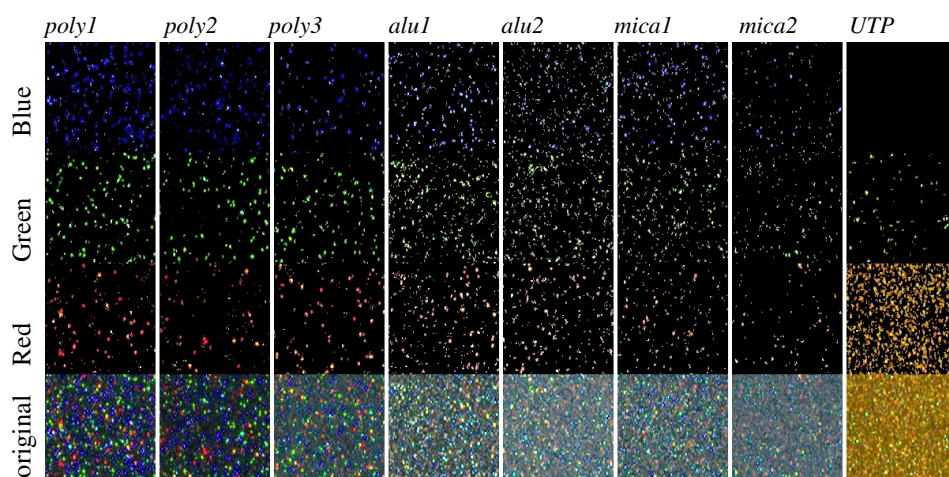
Figure 3: Example of identified flakes in individual RGB color channels for seven effect pigments (out-of-plane geometry and illumination azimuthal angle 230°, area 6×6 mm).

carding all elements with a size smaller than 3 x 3 pixels. Finally, the number of the remaining connected regions and their pixel area are counted. Fig. 3 shows examples of identified pigments in each color channel. The original image is on the bottom.

Once individual pigments are identified in each color channel, we can use this information to derive several computational features. The most straightforward one is the *count* of isolated pigments. The second one is percentage of sample surface the *coverage* by the segmented pigments, while the third one is the average *intensity* of segmented pigments.

Our method depends on three parameters: channels difference threshold d, pixel intensity m, and Gaussian filter variance σ. The first two related to a dynamic range of all acquired images. Their settings was relatively stable in the proximity of the values given above, but they can be adjusted when different coating types or different effect particle sizes are analyzed.
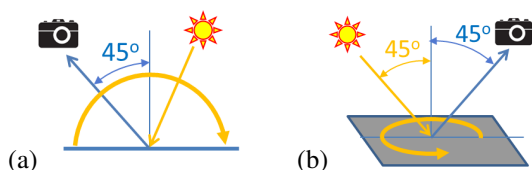
Figure 4: The tested (a) in-plane and (b) out-of-plane illumination/viewing geometry configurations.

5 RESULTS

We performed in-plane and out-of-plane analyses. For in-plane analysis, we used the geometry shown in Fig. 4-a, i.e., with the camera fixed at an elevation angle 45° from the surface normal, while the illumination elevation angles covered the whole plane from -90° to 90°. In the case of the out-of-plane analysis, we had the camera fixed at the same elevation angle 45° from surface normal (Fig. 4-b). The sampling step of measurement for all three geometries was one degree. Please note that both geometries have a blind spot of a span of around 25° due to occlusion of the camera's view by the arm with the light.

The captured in-plane data consisted of 180 images while the out-of-plane data consisted of 360 images of resolution 140×140 pixels corresponding to sample size 6 × 6 mm.

The results of in-plane analysis are shown in Fig. 5-a. The polar graph represents 180° (-90°,90°) covered by images taken over in-plane geometry. For each image the values of pigments count, coverage, and intensity are computed across seven tested materials. The polar plots visualize in-plane geometry laterally and the camera observes material from elevation angle 45° (angle 135° in polar plots). From the plots we can immediately observe noisy behavior of the pigment count (left), which is due to union of isolated pigment flakes, when their intensity increases towards specular highlight. In contrast, the coverage feature (middle) produces more smooth results across entire in-plane geometry, thus allowing clear distinguishing between the tested coatings. By analysis of coverage one can observe that near 20° aspecular (light elevation angle 25°) is a promising candidate for coatings discrimination (shown as angular range denoted as **A**); however, it should be sampled together with around 55° aspecular (light elevation angle -10°) to detect presence of the first order diffraction highlight present for polychromatic coatings (angular range **B**). Further, although the intensity feature
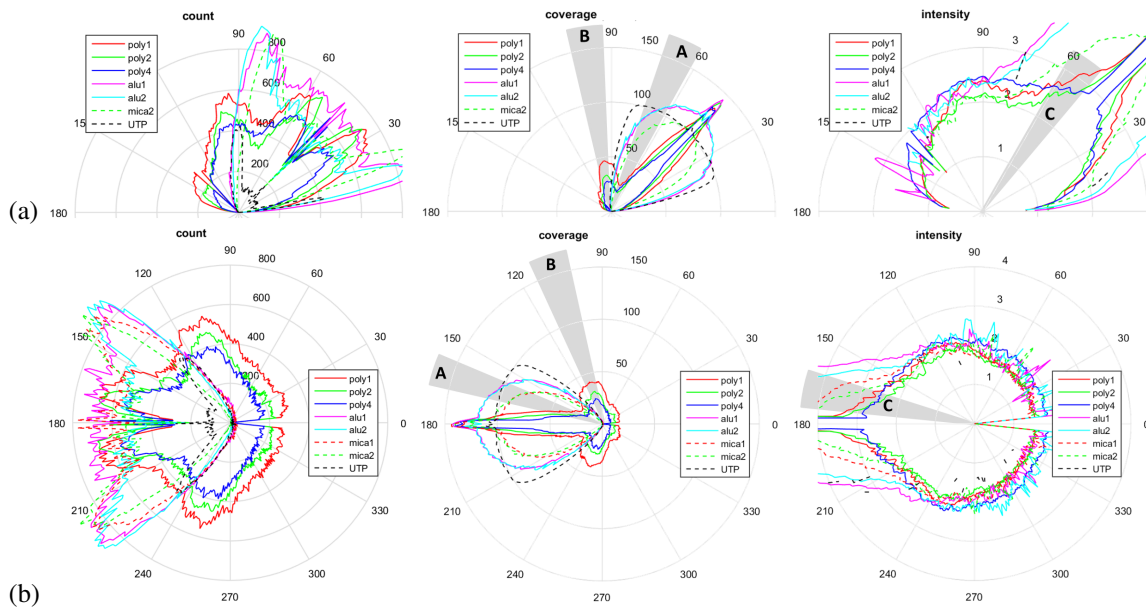
Figure 5: Results of (a) in-plane analysis of seven samples and (b) out-of-plane analysis of eight samples. Segmented pigments count (left), their percentage of sample area coverage (middle), and average intensity (right).

(right) shows relatively noisy behavior too, the angles close to specular reflection allow discrimination between the water/solvent-based coatings technologies (angular range **C**).

The results of out-of-plane analysis are shown in Fig. 5-b. The polar graph represents 360° covered by images taken over out-of-plane geometry. Again, for each image the values of pigments count, coverage, and intensity are computed across eight tested materials. In this case, we observe the geometry from the overhead, where the camera is at azimuth 0°. Different azimuthal illumination directions produce the behavior very similar to the one for the in-plane geometry. Again, the percentage of area coverage produces the smoothest results and optimal discrimination azimuthal angles are near 160° and 200° (denoted by areas **A**) in combination with 100° and 260° (denoted by areas **B**) from a camera azimuth. The intensity image shows a again promising range of angles for coating technologies discrimination denoted as **C**.

In both cases, it is clear that the *coverage* and *intensity* features are able clearly separate not only different coating materials, but also their different variants due to coating technology.

6 SPATIAL UNIFORMITY OF EFFECT PIGMENTS

Finally, we applied the proposed pigment segmentation results to analysis of a spatial uniformity of effect
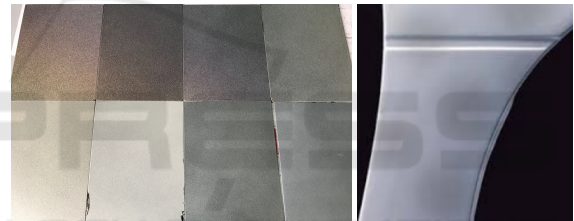
Figure 6: An example of cloudiness / mottling visible as spatial nonuniformity on: (left) a set of coated panels, (right) a part of car body.

coatings. These visually disturbing non-uniform artifacts (see Fig. 6) are in coating industry denotes as cloudiness or mottling. Therefore, their reliable detection is crucial for quality control of coating production process, where non-uniform coating application produces cloudy artifact visible at specific, typically diffuse, illumination conditions. The cloudiness is caused by a coating composition, movement of spray-gun over the coated object, shape of the nozzle, air pressure and other parameters in painting application and solidification process. As such artifacts are often barely visible, one can either rely on a dedicated hardware for cloudiness evaluation or on knowledge of a trained expert. Based on this, the parameters of the coating process are iteratively adjusted till an acceptable coating uniformity is reached.

We tackle this problem by proposing a technique relying on behavior of isolated pigments contours in each captured image described in Section 4. Let *I* be a single RGB image from out-of-plane geom-

etry, $f_B(I_s(i),d,m,\sigma)$ is a function generating binary image containing only pixels indicating presence of segmented flakes in a selected RGB channel s, where d,m,σ are segmentation parameters, and $i \in \{0°,360°\}$ is azimuthal angle across out-of-plane geometry. First, we sum up the detected flakes contribution across all RGB channels to obtain a single binary image

$$A_i = \sum_{s=\{R,G,B\}} f_B\left(I_s(i);d,m,\sigma\right) \ . \quad (3)$$

Then, a *density* map of pigment flakes is obtained as

$$D = \sum_{i=1°}^{360°} A_i \ . \quad (4)$$

As we want also evaluate differences due to non-uniform orientation of pigment flakes we compute also pixel-wise standard variance of pigments presence across different azimuthal angles, we compute a *variation* map as

$$V = \frac{1}{360} \sum_{i=1°}^{360°} (A_i - D)^2 \ . \quad (5)$$

We apply these two features (*density D* and *variance V*) on two effect coatings *mica1, mica2*. As we want to capture also non-uniformity due to pigment disorientation, we decided to use out-of-plane geometry described in Fig. 4-b. Due to optical diffraction effect resulting in limited depth of field for viewing elevation angle 45°, we restricted the region-of-interest in camera direction to guarantee sharp texture across entire analyzed area as shown in Fig. 7-a. The size of analyzed image is 1300×717 pixels corresponding to area 60×30 mm.
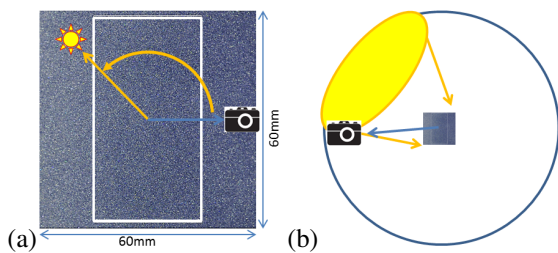
Figure 7: (a) A region of interest selection on the sample plane and its relation to measured out-of-plane geometry, (b) an overhead scheme of illumination and viewing conditions for obtaining cloudiness reference images.

The obtained uniformity maps using both proposed features side-by-side with enhanced photograph of the coated panels are shown in Fig. 8. These reference images (left) were obtained by using quarter-hemisphere diffuse illumination and nearly retro-reflective viewing angle as shown schematically

in Fig. 7-b (light and camera elevation angles are 45° and their distances from the sample are 0.7 m). The original feature images are rather noisy, so we filtered these images using a median filter with a kernel size 100×100 pixels. The filtered images on the right can be regarded as uniformity maps, highlighting differences between spatial locations due to a different density of detected pigment flakes. The black banding is due to the filter kernel size. When comparing the results to the reference image on the left, we can observe, that although both features correlate with the reference, a slightly better performance in non-uniformity prediction was obtained using the density feature. Fig. 8 also shows a dynamic range of values in non-uniformity maps for both tested materials and features. Higher values for *mica1* are due to a higher contrast in flakes structure.

7 CONCLUSION

We proposed a gonioapparent effect coatings characterization method based on using a total area occupied by pigment flakes at a given image threshold level. Our analysis has shown that the proposed method is able to clearly distinguish pigment materials and coating applications in both in-plane and out-of-plane geometries. Results also revealed that one can identify a sparse set of geometries that perform the best in differentiation of the coatings materials and different coating technology. These geometries can be used to obtain complementary information to that obtained by commercial instruments and can be regarded as possible measurement geometry candidates for future instruments. Finally, we have shown application of our image segmentation results over out-of-plane geometry, to assessment of coating spatial non-uniformity, i.e. cloudiness or mottling, of effect coatings. To sum up, our results show that using gonioapparent image-based data is a promising way of effective and reliable characterization of effect coatings as well as for pigment spatial uniformity analysis. In future, we plan to derive a computational measure of spatial non-uniformity of effect coatings based on combination of uniformity map histogram and frequency analysis.

ACKNOWLEDGMENT

(a) reference photo   (b) *density*   filtered   (c)*variance*   filtered
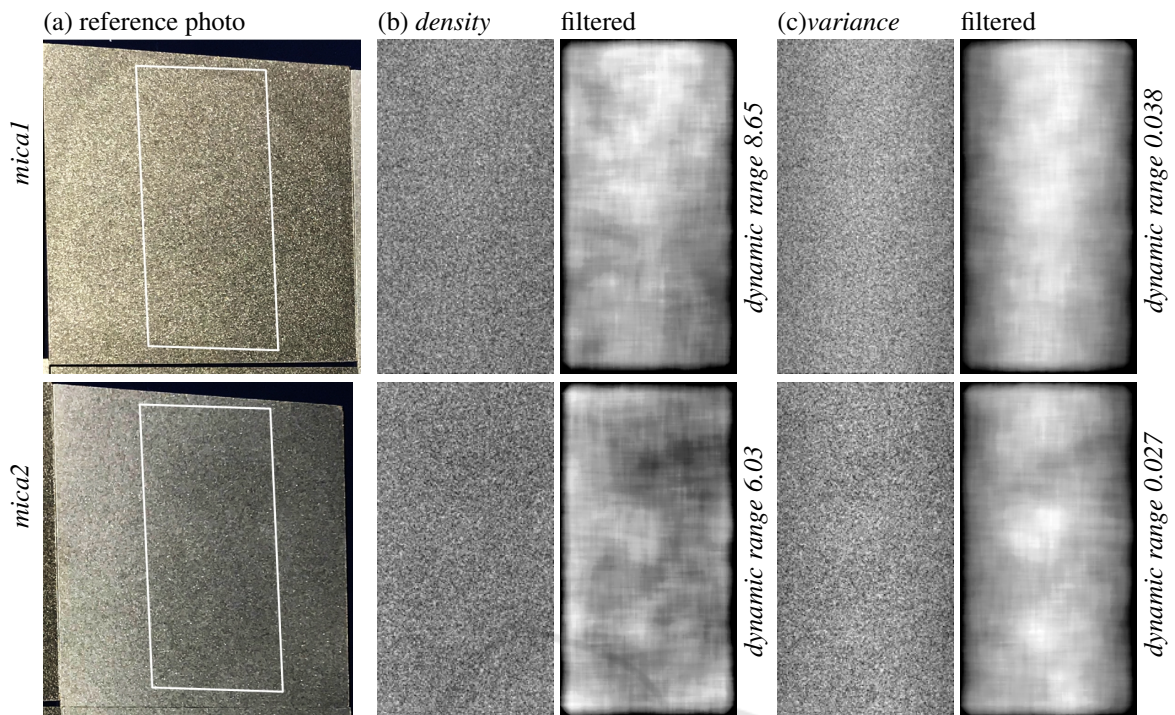
Figure 8: Results of out-of-plane spatial uniformity analysis of samples *mica1* and *mica2*: (a) reference cloudiness obtained by SW enhancement of the coated panel photograph, (b,c) results of the density *D* and variance *V* features, respectively, and their filtering using median filter. Dynamic ranges of individual features are included.

REFERENCES

(1999). Deutsches Institut für Normung e.V., DIN 55945.

Dana, K., van Ginneken, B., Nayar, S., and Koenderink, J. (1999). Reflectance and texture of real-world surfaces. *ACM Transactions on Graphics*, 18(1):1–34.

E2194-12, A. (2012). Standard practice for multiangle color measurement of metal flake pigmented materials. *West Consh. PA: ASTM Inter., 2012*.

E2539-12, A. (2012). Standard practice for multiangle color measurement of interference pigments. *West Conshohocken PA: ASTM Inter., 2012*.

Ferrero, A., Bernad, B., Campos, J., Perales, E., Velázquez, J. L., and Martínez-Verdú, F. M. (2016). Color characterization of coatings with diffraction pigments. *JOSA A*, 33(10):1978–1988.

Ferrero, A., Campos, J., Perales, E., Martínez-Verdú, F. M., Van der Lans, I., and Kirchner, E. (2015). Global color estimation of special-effect coatings from measurements by commercially available portable multiangle spectrophotometers. *Journal of the Optical Society of America A*, 32(1):1–11.

Ferrero, A., Rabal, A., Campos, J., Martínez-Verdú, F., Chorro, E., Perales, E., Pons, A., and Hernanz, M. L. (2013). Spectral brdf-based determination of proper measurement geometries to characterize color shift of special effect coatings. *Journal of the Optical Society of America A*, 30(2):206–214.

Filip, J., Vávra, R., Haindl, M., Zid, P., Krupicka, M., and Havran, V. (2013). BRDF slices: Accurate adaptive anisotropic appearance acquisition. In *Conference on Computer Vision and Pattern Recognition*, pages 4321–4326.

Gómez, O., Perales, E., Chorro, E., Burgos, F. J., Viqueira, V., Vilaseca, M., Martínez-Verdú, F. M., and Pujol, J. (2016). Visual and instrumental assessments of color differences in automotive coatings. *Color Research & Application*, 41(4):384–391.

Höpe, A., Koo, A., Verdu, F. M., Leloup, F., Obein, G., Wübbeler, G., Campos, J., Iacomussi, P., Priit, J., and Källberg, S. (2014). Multidimensional reflectometry for industry (xd-reflect) a european research project. In *Electronic Imaging*, number 9018-04, pages 1–11.

Hunter, R. S. (1937). Methods of determining gloss. *NBS Research paper RP*, 958.

Kim, D. B., Seo, M. K., Kim, K. Y., and Lee, K. H. (2010). Acquisition and representation of pearlescent paints using an image-based goniospectrophotometer. *Optical engineering*, 49(4):043604.

Kirchner, E. and Cramer, W. (2012). Making sense of measurement geometries for multi-angle spectrophotometers. *Color Research & Application*, 37(3):186–198.

Lans, I. v. d., Kirchner, E., and Half, A. (2012). Accurate appearance-based visualization of car paints. In *Proceedings of International Conference on Computer Graphics*, volume 2012, pages 17–23.

Maile, F. J., Pfaff, G., and Reynders, P. (2005). Effect pig-

ment – past, present and future. *Progress in Organic Coatings*, 54(3):150 – 163.

Maile, F. J. and Reynders, P. (2010). A colorful menagerie of platelets for transparent effect pigments. *Asia Pacific Coatings Journal*, 23(1):14–17.

McCamy, C. (1996). Observation and measurement of the appearance of metallic materials. part i. macro appearance. *Color Research & Application*, 21(4):292–304.

Mihálik, A. and Ďurikovič, R. (2013). Metallic paint appearance measurement and rendering. *Journal of Applied Mathematics, Statistics and Informatics*, 9(2):25–39.

Nicodemus, F., Richmond, J., Hsia, J., Ginsburg, I., and Limperis, T. (1977). Geometrical considerations and nomenclature for reflectance. *NBS Monograph 160*, pages 1–52.

Perales, E., Chorro, E., Viqueira, V., and Martínez-Verdú, F. M. (2013). Reproducibility comparison among multiangle spectrophotometers. *Color Research & Applications*, 38(3):160–167.

Pfaff, G. (2008). *Special effect pigments: technical basics and applications*. Vincentz Network GmbH & Co KG, Hannover.

Pfaff, G. and Reynders, P. (1999). Angle-dependent optical effects deriving from submicron structures of films and pigments. *Chemical reviews*, 99(7):1963–1982.

Rump, M., Sarlette, R., and Klein, R. (2009). Efficient resampling, compression and rendering of metallic and pearlescent paint. In Magnor, M., Rosenhahn, B., and Theisel, H., editors, *Vision, Modeling, and Visualization*, pages 11–18.

Strothkämper, C., Hauer, K.-O., and Höpe, A. (2016). How to efficiently characterize special effect coatings. *Journal of the Optical Society of America A*, 33(1):1–8.